Variance Distribution of Five Global Precipitation Sets

Alex C. Ruane (aruane@ucsd.edu)
John O. Roads (jroads@ucsd.edu)
Experimental Climate Prediction Center
Scripps Institution of Oceanography / UCSD

1. Introduction

- Variance distributions of precipitation from two global models and three satellite-derived precipitation sets are calculated from 6-hour to annual periods. Despite improving skill in the observation and simulation of precipitation's long-term means, the temporal statistics at which precipitation falls is still not handled accurately. Distinct physical mechanisms govern the distribution of variance across many temporal scales, and the ability of global reanalyses to distribute precipitation accordingly is a challenging test of a model's hydrometeorology. Physical parameterizations and land-surface schemes are especially vulnerable to errors in variance distribution. Results from this study are in press at the Earth Interactions Journal (Ruane and Roads, 2007b).

2. Datasets

Precipitation sets from two types of sources are examined in this study, although all sets contain 3-hourly resolution:

- High Resolution Precipitation Products (HRPPs) utilize innovative algorithms to dynamically and statistically process observations from geostationary and low-orbitting satellites, producing gridded precipitation data at high temporal and spatial resolution. Data from the Tropical Rainfall Measuring Mission's 3B-42 product (TRMM 3B-42; see http://trmm.gsfc.nasa.gov/3b42.html and Adler et al., 1994), the Climate Prediction Center's Morphing Method (CMORPH; Joyce et al., 2004), and the Precipitation Estimation from Remotely Sensed Information using Artificial Neural Networks (PERSIANN; Hsu et al., 1997) were evaluated at 1-degree resolution. HRPP coverage is limited to lower latitudes due to the orbital patterns of microwave sensors. This study is one of the first intercomparisons of the HRPPs' temporal characteristics. CMORPH data is not available until the end of 2002, so CMORPH evaluations examine the 2003-2005 period as opposed to the 2002-2004 period that is examined in the other four sets and coincides with data created for the Coordinated Enhanced Observing Period (CEOP, Koike, 2004).
- Augmented 6-hour forecasts were initialized four times each day (at 00, 06, 12, and 18UTC) during the CEOP period for the NCEP/Department of Energy Reanalysis-2 (RII, Kanamitsu et al., 2002b) as well as the Seasonal Forecast Model (SFM, Kanamitsu et al., 2002a) reanalysis. Detailed model descriptions are available in Ruane and Roads, 2007a. For this study, a 3-hourly time series of precipitation is generated by linking together successive 3- and 6-hour forecasts from each augmented run; each forecast representing the average precipitation rate during the three preceding hours. Global reanalysis features coarser output resolution (~1.9x1.875 degrees) and are driven by sea-surface temperatures which lack diurnal variation.

3. Methodology

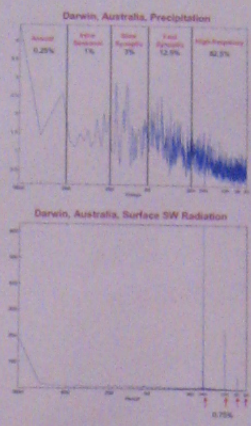

- Three-hourly time series of precipitation from three high resolution precipitation products (TRMM 3B-42, CMORPH, and PERSIANN) and two reanalyses are examined for their frequency characteristics using broad and narrow variance categories. After defining the diurnally forced spectral peaks (at 24, 12, 8, and 6 hours) by examining the solar signal, the power spectra are divided into comprehensive broad bands comprising the annual (80 days - 1 year), intraseasonal (20-80 days), slow (6-20 days) and fast (6-36 days) synoptic, and high-frequency (6-36 hours) periods. Global maps accounting for 100% of precipitation's variance are analyzed to identify unique regional behaviors.
- Annual Band: 80 days – 1 year. Captures seasonal shifts, monsoons, and the migration of the ITCZ.
- Intraseasonal Band: 20-80 days. Contains both modeled and observed Madden-Julian oscillations (Madden and Julian, 1994).
- Slow Synoptic Band: 6-20 days. Captures range of slow moving or long-lasting synoptic waves.
- Fast Synoptic Band: 36 hours – 6 days. Displays fast moving or short-lived Rossby and inertio-gravity waves.
- High-Frequency Bands: 6-36 hours with the exception of the diurnal bands. Captures mesoscale activity and rapid transitions of atmospheric structure.
- Diurnal Category: Narrow bands centered on 24-, 12-, 8-, and 6-hour periods. Captures the mean diurnal cycle of precipitation.
- These variance categories are not of equal width, so the percentage variance that would be expected from a random signal is listed with each map as a reference. Spectra that could not be distinguished from a random variable spectrum were omitted.

4. CMORPH Detail

- The comprehensive variance maps from CMORPH are shown in this section to demonstrate the types of features seen throughout the five precipitation sets. Please note that the colorbars vary between maps.

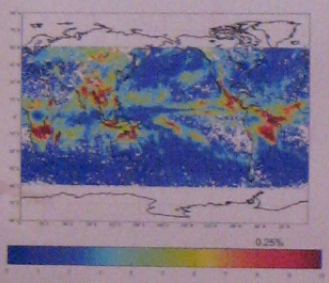

Annual Percentage Variance

– Monsoonal rain patterns and the seasonal shift of the ITCZ far exceed the variance expected from a random variable. The East Pacific Rossby wave trains are also apparent.

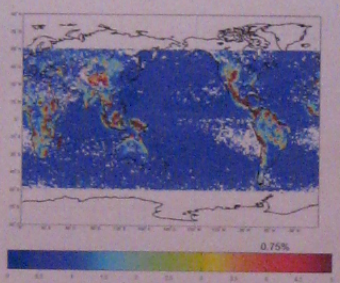

Diurnal Percentage Variance

– Mountains, coastlines, and tropical land masses show the highest percentage of diurnal variance. Places containing all three are well above the expected value.

– The high values in the Western U.S. are notable for their amplitude, but do not indicate phase information.

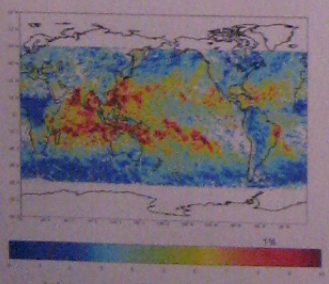

Intraseasonal Percentage Variance

– The highest percentages of variance in this category are over warm, off-equatorial water, particularly in the Indo-Pacific region known for Madden-Julian Oscillation activity.

– Equatorial variance is spread amongst the variance categories at higher frequencies, as precipitation driven by large-scale forcing may arrive through higher-frequency mechanisms.

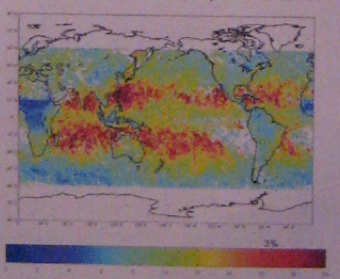

Slow Synoptic Percentage Variance

– Slow Synoptic variance tends to be most influential in areas that feature large-scale subsidence (between 20-30° N/S; also note subtle maxima in some arid regions). Mean precipitation in these regions is low, but rainfall arrives when strong synoptic systems or low-level atmospheric "rivers" penetrate the stable environments and last for an extended period of time.

Fast Synoptic Percentage Variance

– Higher percentages over ocean than land indicate fast synoptic waves are better able to maintain their structure over the relatively consistent ocean surface.

– Model drawn have a stronger signal, suggesting a role for moisture recycling in maintaining a precipitating system.

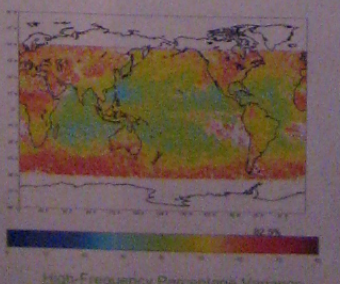

High-Frequency Percentage Variance

– Higher percentages over land stem from large gradients in topography, moisture, vegetation, and soil types lead to high frequency variations in propagating storms.

– This is the only category that is consistently below the random variable's expected variance, indicating a red spectrum for precipitation.

5. Intraseasonal Comparison

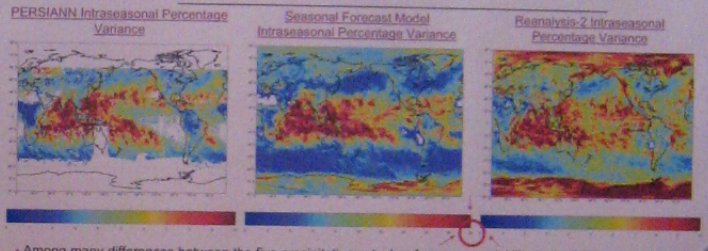

- Among many differences between the five precipitation sets, low-frequency variability in the SFM reanalysis was considerably stronger than in any other global set (note that the colorbar limits above are twice as high as those of the other sets), likely due to the use of the Relaxed Arakawa-Schubert convective parameterization (Moorthi and Suarez, 1992).
- Among other notable differences:
  1) Stronger high-frequency variance in TRMM 3B-42 than in other HRPP.
  2) Weaker Land-sea contrast in SFM reanalysis than in RII.

6. Zonal Means

- Zonal mean averages of the percentage variance displayed by each variance categories are displayed in this section for each precipitation set. Land (solid line) and sea (dashed line) points are separated for each category.
  - A clear land sea contrast is evident in all precipitation sets, although it is weakest in the SFM. Low-frequency variance categories display higher variance over the ocean, while high-frequency variation is strongest over the land.
  - The reanalysis models demonstrate more meridional variation than the HRPPs.
  - Low-frequency variance is heightened in the SFM at the expense of the higher frequency variance, particularly in the Tropics.
  - TRMM 3B-42 variance is least distinguishable from the random variable spectrum.

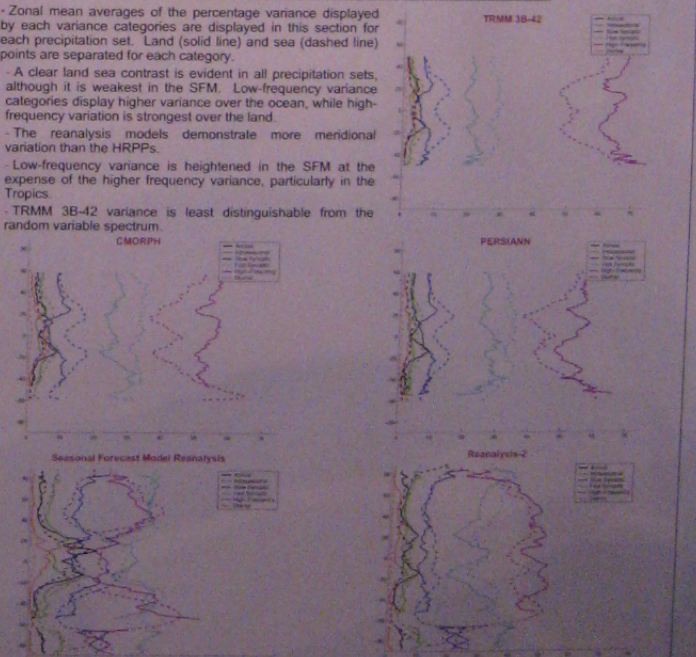

References

Adler, R.F., G.J. Huffman, and P.R. Keehn, 1994: Global rain estimates from microwave adjusted geosynchronous IR data. Remote Sens. Rev., 11, 125-152.

Hsu, K., X. Gao, S. Sorooshian, and H.V. Gupta, 1997: Precipitation estimation from remotely sensed information using artificial neural networks. J. Appl. Meteor., 36, 1176-1190.

Joyce, R.J., J.E. Janowiak, P.A. Arkin, and P. Xie, 2004: CMORPH: A method that produces global precipitation estimates from passive microwave and infrared data at high spatial and temporal resolution. J. Hydrometeorology, 5, 487-503.

Kanamitsu, M., W. Ebisuzaki, J. Woollen, S.-K. Yang, J. Hnilo, M. Fiorino, and J. Potter, 2002a: NCEP/DOE AMIP-II Reanalysis (R-2). Bull. Amer. Meteor. Soc., 83(11), 1631-1643.

Kanamitsu, M., A. Kumar, H.-M.H. Juang, J.-K. Schemm, W. Wang, F. Yang, S.-Y. Hong, P. Peng, W. Chen, S. Moorthi, and M. Ji, 2002b: NCEP dynamical seasonal forecast system 2000. Bull. Amer. Meteor. Soc., 83(7), 1019-1037.

Koike, T., 2004: The Coordinated Enhanced Observing Period – an initial step for integrated global water cycle observation. WMO Bulletin, 53(3).

Madden, R.A., and R.H. Julian, 1994: Observations of the 40-50-day tropical oscillation – A review. Mon. Wea. Rev., 122, 814-837.

Moorthi, S., and M.J. Suarez, 1992: Relaxed Arakawa-Schubert: A parameterization of moist convection for general circulation models. Mon. Wea. Rev., 120, 978-1002.

Ruane, A.C., and J.O. Roads, 2007a: The diurnal cycle of water and energy over the contiguous United States from three reanalyses. J. Hydrol. Eng., 12(2), 116-130.

Ruane, A.C., and J.O. Roads, 2007b: 6-hour to 1-year variance of five global precipitation sets. Earth Interactions, submitted.